CHIN. PHYS. LETT. Vol. 38, No. 7 (2021) 077402 **Express Letter**

S-Wave Superconductivity in Kagome Metal CsV_3Sb_5 Revealed by $^{121/123}$Sb NQR and ^{51}V NMR Measurements

Chao Mu(牟超)[1,2], Qiangwei Yin(殷蔷薇)[3], Zhijun Tu(涂志俊)[3], Chunsheng Gong(龚春生)[3], Hechang Lei(雷和畅)[3], Zheng Li(李政)[1,2*], and Jianlin Luo(雒建林)[1,2,4*]

[1]*Beijing National Laboratory for Condensed Matter Physics and Institute of Physics, Chinese Academy of Sciences, Beijing 100190, China*

[2]*School of Physical Sciences, University of Chinese Academy of Sciences, Beijing 100190, China*

[3]*Department of Physics and Beijing Key Laboratory of Opto-electronic Functional Materials & Micro-nano Devices, Renmin University of China, Beijing 100872, China*

[4]*Songshan Lake Materials Laboratory, Dongguan 523808, China*

(Received 9 June 2021; accepted 28 June 2021; published online 30 June 2021)

We report $^{121/123}$Sb nuclear quadrupole resonance (NQR) and ^{51}V nuclear magnetic resonance (NMR) measurements on kagome metal CsV_3Sb_5 with $T_c = 2.5$ K. Both ^{51}V NMR spectra and $^{121/123}$Sb NQR spectra split after a charge density wave (CDW) transition, which demonstrates a commensurate CDW state. The coexistence of the high temperature phase and the CDW phase between 91 K and 94 K manifests that it is a first-order phase transition. At low temperature, electric-field-gradient fluctuations diminish and magnetic fluctuations become dominant. Superconductivity emerges in the charge order state. Knight shift decreases and $1/T_1T$ shows a Hebel–Slichter coherence peak just below T_c, indicating that CsV_3Sb_5 is an s-wave superconductor.

DOI: 10.1088/0256-307X/38/7/077402

Kagome lattice has been intensely studied in condensed matter physics due to its geometric frustration and nontrivial band topology. Depending on the electron filling, on-site repulsion U, and nearest-neighbor Coulomb interaction V, several possible states have been proposed as the ground state,[1,2] such as quantum spin liquid,[3–5] charge density wave (CDW),[6] and superconductivity.[7,8]

Recently, superconductivity was discovered in the kagome metal AV_3Sb_5 (A = K, Rb, Cs), which undergoes a CDW transition before the superconducting transition.[9–12] Scanning tunneling microscopy (STM) observed a chiral charge order that breaks time-reversal symmetry[13] and leads to the anomalous Hall effect in the absence of magnetic local moments.[14–17] This chiral charge order is energetically preferred and tends to yield orbital current.[18] Inelastic x-ray scattering and Raman scattering exclude strong electron-phonon coupling driven CDW,[19] while optical spectroscopy supports that CDW is driven by nesting of Fermi surfaces.[20] High pressure can suppress CDW transition and reveal a superconducting dome in the P–T phase diagram.[21,22] Further increasing pressure, a new superconducting phase emerges.[23–25]

STM studies observed possible Majorana modes[26] and pair density wave,[27] which points to unconventional superconductivity in the surface state. Signatures of spin-triplet pairing and an edge supercurrent have been observed in $Nd/K_{1-x}V_3Sb_5$ devices.[28] Whether the exotic surface superconducting state is intrinsic or comes from heterostructures, such as $Bi_2Te_3/NbSe_2$,[29] needs to clarify the gap symmetry in the bulk state first. Thermal conductivity measurements on CsV_3Sb_5 down to 0.15 K showed a finite residual linear term, which suggests a nodal gap and points to unconventional superconductivity.[25] On the other hand, magnetic penetration depth of CsV_3Sb_5 measured by tunneling diode oscillator showed a clear exponential behavior at low temperatures, which provides an evidence for nodeless superconductivity but does not rule out fully gapped unconventional superconductivity.[30]

In this work, we report nuclear magnetic resonance (NMR) and nuclear quadrupole resonance (NQR) investigations on CsV_3Sb_5. The splitting of ^{51}V spectra and $^{121/123}$Sb spectra demonstrates that a commensurate CDW order forms at 94 K with a first-order transition and coexists with superconductivity. In the superconducting state, Knight shift decreases and a Hebel–Slichter coherence peak appears in the spin-lattice relaxation rate just below T_c, which provides evidences for s-wave superconductivity in CsV_3Sb_5.

Single crystals of CsV_3Sb_5 were synthesized using the self-flux method, as reported in Ref. [21]. Superconductivity with $T_c = 2.5$ K is confirmed by dc magnetization measured using a superconducting quantum interference device (SQUID). The NMR

Supported by the National Key Research and Development Program of China (Grant Nos. 2017YFA0302901, 2018YFE0202600, and 2016YFA0300504), the National Natural Science Foundation of China (Grant Nos. 11921004, 11634015, 11822412, and 11774423), the Beijing Natural Science Foundation (Grant No. Z200005), and the Strategic Priority Research Program and Key Research Program of Frontier Sciences of the Chinese Academy of Sciences (Grant No. XDB33010100).

*Corresponding authors. Email: lizheng@iphy.ac.cn; jlluo@iphy.ac.cn

© 2021 Chinese Physical Society and IOP Publishing Ltd

and NQR measurements were performed using a phase coherent spectrometer. The spectra were obtained by frequency step and sum method which sums the Fourier transformed spectra at a series of frequencies.[31] The spin-lattice relaxation time T_1 was measured using a single saturation pulse.

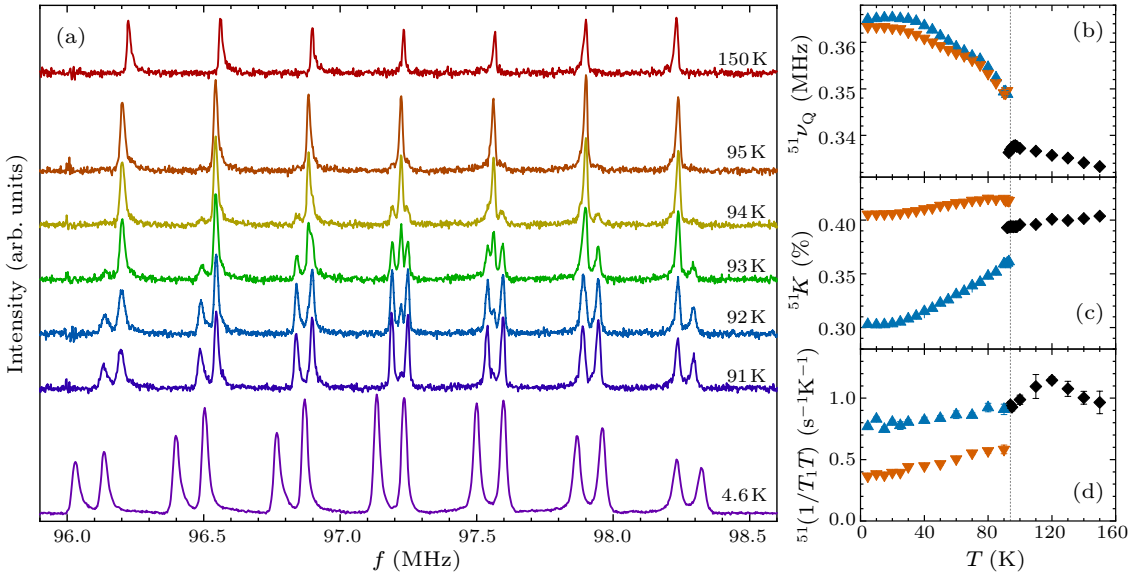

Fig. 1. (a) ^{51}V-NMR spectra with $H \parallel c$. (b) Temperature dependence of quadrupole resonance frequency ν_Q. (c) Temperature dependence of the Knight shift of ^{51}V. (d) Temperature dependence of the $^{51}(1/T_1T)$ measured at the central peaks. The vertical dashed line indicates the position of T_{CDW}.

Figure 1(a) shows the spectra of ^{51}V with $\mu_0 H$ (= 8.65 T) $\parallel c$. ^{51}V with $I = 7/2$ has seven NMR peaks at 150 K. Below $T_{CDW} = 94$ K, the magnitude of original peaks decreases gradually and two sets of new peaks arise, which indicates that the CDW transition is commensurate and there are two different sites of V atoms in the CDW state. The coexistence of two phases between 91 K and 94 K demonstrates that the CDW transition is of first-order due to a simultaneous superlattice transition.[10] The quadrupole resonance frequencies of both ^{51}V sites increase with decreasing temperature below 94 K, as shown in Fig. 1(b).

Knight shift ^{51}K is deduced from the central peaks and is summarized in Fig. 1(c). Below T_{CDW}, two splitting peaks give two Knight shift values, one of which jumps up and the other jumps down. The corresponding $^{51}(1/T_1T)$ jumps to the opposite side or does not change at T_{CDW}, as shown in Fig. 1(d). We also measured the Knight shift and $^{51}(1/T_1T)$ with $H \perp c$, as shown in Fig. S1 of the Supplemental Material, which also shows an opposite trend at T_{CDW}. Therefore, the splitting of ^{51}K is not caused by different hyperfine couplings, but by the change of the orbital part of Knight shift.

$^{51}(1/T_1T)$ in a Fermi liquid state is proportional to the square of the density of states (DOS) around the Fermi energy $N(E_F)$. Just below T_{CDW}, $^{51}(1/T_1T)$ of the right peak jumps to 64% of the value above T_{CDW}, indicative of the decrease of $N(E_F)$ by 20%. $^{51}(1/T_1T)$ of the left peak is smooth at T_{CDW}. The difference of $^{51}(1/T_1T)$ between two V sites manifests the modulation of DOS at different V positions, which is consistent with 2×2 CDW charge order.[27] ^{51}V has a very small quadrupole moment, $Q = -5.2 \times 10^{-30}$ m^2. Therefore, the relaxation is governed by magnetic fluctuations and can reflect the change in the DOS, even though the electric field gradient (EFG) fluctuates strongly near T_{CDW}. On the contrary, ^{121}Sb and ^{123}Sb have larger quadrupole moments, $^{121}Q = -54.3 \times 10^{-30}$ m^2 and $^{123}Q = -69.2 \times 10^{-30}$ m^2, respectively, which can be used to detect the EFG fluctuations and perform NQR measurement.

In order to study the superconducting state, we must perform measurement at a magnetic field lower than the upper critical field, $\mu_0 H_{c2} \sim 0.5$ T.[25] Usually NQR experiments do not need applying magnetic field, however Knight shift cannot be measured at zero field. Here we measure ^{121}K by applying a perturbing field of 64 Oe that is larger than the lower critical field, $\mu_0 H_{c1} \sim 2$ mT.[32] With a perturbing field, the nuclear spin Hamiltonian is the sum of electric quadrupole interactions and the nuclear Zeeman energy[33]

$$\begin{aligned}\mathcal{H} &= \mathcal{H}_Q + \mathcal{H}_Z \\ &= \frac{h\nu_{zz}}{6}\left[(3I_z^2 - I^2) + \frac{\eta(I_+^2 + I_-^2)}{2}\right] \\ &\quad -\gamma\hbar(1+K)H_0\left(I_z\cos\theta + \frac{I_+e^{-i\phi} + I_-e^{i\phi}}{2}\sin\theta\right). \quad (1)\end{aligned}$$

Here ν_{zz} is the quadrupole resonance frequency along the principal axis (c-axis), $\nu_{zz} \equiv \frac{3e^2qQ}{2I(2I-1)}$, with $eq = V_{zz}$; η is an asymmetry parameter of the EFG, $\eta = \frac{V_{xx} - V_{yy}}{V_{zz}}$. V_{xx}, V_{yy}, V_{zz} are the EFGs along the x, y, z directions, respectively; θ and ϕ are the polar and

azimuthal angles between the direction of the applied field and the principal axis of EFG. When η is small enough to be negligible, the resonance frequency at a small perturbation field along c-axis is

$$\nu_{\rm NQR}(H_0) = \nu_{\rm NQR}(0) \mp \gamma(1+K)H_0,\ I_z = \pm|I_z|. \quad (2)$$

The perturbing field eliminates the degeneration of $\pm I_z$ and results in a spectra splitting. When $H_0 \perp c$, the peak of $|\pm\frac{1}{2}\rangle \leftrightarrow |\pm\frac{3}{2}\rangle$ is split by the perturbing field, while other peaks are not affected.[34]

$$\nu_{\rm NQR}(H_0) = \nu_{\rm NQR}(0) \pm \frac{I+\frac{1}{2}}{2}\gamma(1+K)H_0, \quad |\pm\frac{1}{2}\rangle \leftrightarrow |\pm\frac{3}{2}\rangle,$$
$$\nu_{\rm NQR}(H_0) = \nu_{\rm NQR}(0), \quad |\pm m\rangle \leftrightarrow |\pm(m+1)\rangle,\ m \geq \frac{3}{2}, \quad (3)$$

where m is a half-integer.

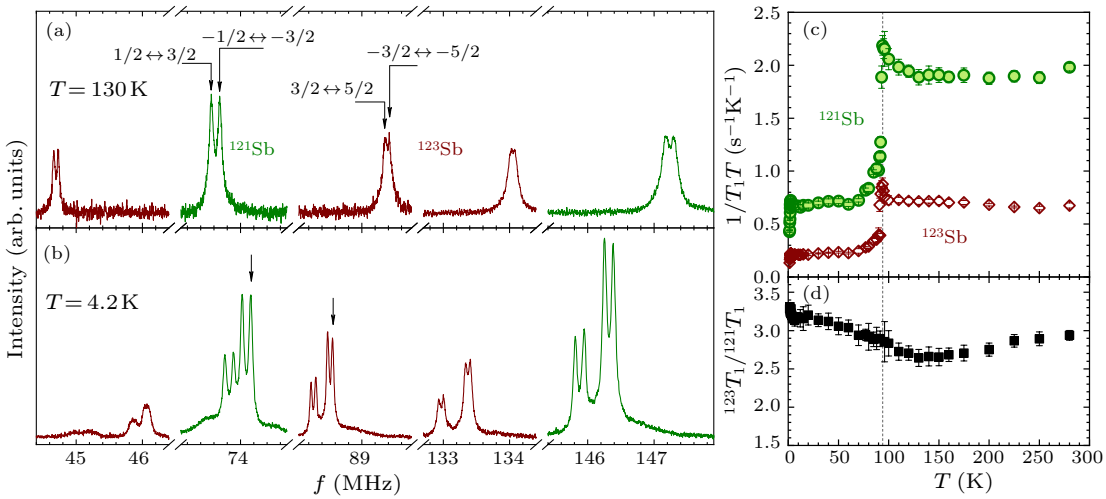

Fig. 2. $^{121/123}$Sb NQR spectra with a perturbing field of 64 Oe along c-axis at (a) 130 K and (b) 4.2 K, respectively. The arrows mark the peaks where T_1 was measured. (c) Temperature dependence of the $1/T_1T$ measured with ^{121}Sb at $-1/2 \leftrightarrow -3/2$ peak and ^{123}Sb at $-3/2 \leftrightarrow -5/2$ peak, respectively. (d) Temperature dependence of the $^{121/123}$Sb isotopic ratio $^{123}T_1/^{121}T_1$. The vertical dashed line indicates the position of $T_{\rm CDW}$.

There are two isotopes of Sb nuclei which are ^{121}Sb with $I = 5/2$ and ^{123}Sb with $I = 7/2$. The NQR spectra should contain two ^{121}Sb peaks and three ^{123}Sb peaks. Figures 2(a) and 2(b) show the spectra with a perturbing field of 64 Oe along c-axis, which eliminates the degeneration of $\pm I_z$ and results in a small spectral splitting. There are two different crystallographic sites for Sb in CsV_3Sb_5 with the atomic ratio of Sb1 : Sb2 = 1 : 4.[9] The relative intensities of different sites are proportional to their atomic ratio,[35] so Sb2 site has larger spectral intensity than Sb1 site. The spectra in Figs. 2(a) and 2(b) are of Sb2 atoms which encapsulate the kagome layer with a graphite-like network. Sb1 atoms located in the kagome plane with V atoms have weak spectra, which are presented in the Supplemental Material. The ν_{zz} and η deduced from the spectra above and below $T_{\rm CDW}$ are summarized in Table 1, where η is zero above $T_{\rm CDW}$ reflecting isotropy in the xy-plane. Below $T_{\rm CDW}$, η of Sb2 changes to finite values, which indicate the breaking of in-plane symmetry and two unequal sites of Sb2 with the ratio of 1 : 2. The slightly decreasing ν_{zz} implies that the main change is not the EFG strength, but the EFG direction at Sb2 sites. On the other hand, the EFG at Sb1 site changes frequency obviously without asymmetry.

Table 1. The quadrupole resonance frequencies and asymmetry parameters.

T	Site	η	$^{121}\nu_{zz}$	$^{123}\nu_{zz}$
130 K	Sb1	0	71.41	43.35
	Sb2	0	73.62	44.69
4.2 K	Sb1	0	78.19	47.16
	Sb2′	0.097	73.08	44.36
	Sb2″	0.099	73.31	44.50

T_1 was measured at $|-\frac{1}{2}\rangle \leftrightarrow |-\frac{3}{2}\rangle$ peak of ^{121}Sb2 and $|-\frac{3}{2}\rangle \leftrightarrow |-\frac{5}{2}\rangle$ peak of ^{123}Sb2, respectively. After spectra splitting below $T_{\rm CDW}$, T_1 was measured at the right-side peaks, marked by arrows in Fig. 2(b). The degeneration is eliminated by the magnetic field, so the NQR recovery curves are no longer applicable. The recovery curve used for $|-\frac{1}{2}\rangle \leftrightarrow |-\frac{3}{2}\rangle$ transition of ^{121}Sb is

$$1 - \frac{M(t)}{M(\infty)} = \frac{1}{35}e^{-\frac{t}{T_1}} + \frac{3}{56}e^{-\frac{3t}{T_1}} + \frac{1}{40}e^{-\frac{6t}{T_1}} + \frac{25}{56}e^{-\frac{10t}{T_1}} + \frac{25}{56}e^{-\frac{15t}{T_1}}. \quad (4)$$

The recovery curve used for $|-\frac{3}{2}\rangle \leftrightarrow |-\frac{5}{2}\rangle$ transition

of ^{123}Sb is

$$1-\frac{M(t)}{M(\infty)}=\frac{1}{84}e^{-\frac{t}{T_1}}+\frac{1}{21}e^{-\frac{3t}{T_1}}+\frac{1}{132}e^{-\frac{6t}{T_1}}+\frac{25}{308}e^{-\frac{10t}{T_1}}+\frac{100}{273}e^{-\frac{15t}{T_1}}+\frac{49}{132}e^{-\frac{21t}{T_1}}+\frac{49}{429}e^{-\frac{28t}{T_1}}. \quad (5)$$

We use the same fitting function for both above and below $T_{\rm CDW}$, since the η is small. Figure 2(c) shows the temperature dependence of $1/T_1T$ of $^{121/123}$Sb. Upon cooling, $^{121/123}(1/T_1T)$ starts to increase a little and drops sharply below $T_{\rm CDW}$ for both ^{121}Sb and ^{123}Sb. With further cooling, $^{121/123}(1/T_1T)$ becomes constant from 70 K to $T_{\rm c}$, which obeys the Korringa relation and suggests that the system is in a Fermi liquid state. $^{51}(1/T_1T)$ of ^{51}V has shown that DOS loss is only 20%. Here the large drop implies that the EFG fluctuations play an important role above $T_{\rm CDW}$ and are suppressed after CDW transition. Moreover, $^{121/123}(1/T_1T)$ decreases continuously without sudden jump like $^{51}(1/T_1T)$. This implies that the superlattice transition has strong effect on V atoms that locate in the kagome plane, but has very small effect on Sb2 atoms that locate outside the kagome plane. Therefore, $^{121/123}(1/T_1T)$ of Sb2 shows a second-order CDW transition behavior.

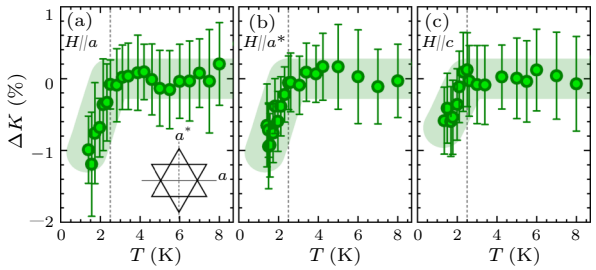

Fig. 3. Temperature dependence of ΔK of ^{121}Sb with (a) $H \parallel a$, (b) $H \parallel a^*$, and (c) $H \parallel c$, where a and a^* are orthogonal directions in the basal plane. The vertical dashed lines indicate the position of $T_{\rm c}$.

In general, a spin-lattice relaxation occurs through magnetic and/or electric-quadrupole channels. The magnetic relaxation is related to the gyromagnetic ratio γ_n and gives $^{123}T_1/^{121}T_1 = 3.4$, while the electric-quadrupole relaxation is related to the quadruple moment Q and gives $^{123}T_1/^{121}T_1 = 1.5$.[36] Above $T_{\rm CDW}$, $^{123}T_1/^{121}T_1$ is smaller than 3, as shown in Fig. 2(d), which indicates that both magnetic fluctuations and EFG fluctuations are important. Below $T_{\rm CDW}$, the ratio increases with decreasing temperature and approaches to 3.4 at zero temperature limit, which indicates that the magnetic process becomes dominant at low temperature. Therefore, the effect of EFG fluctuations in the superconducting state is negligible.

The Knight shift of Sb can be deduced from the spectra splitting. The field calibrated by a Gauss meter has an uncertainty, so the absolute Knight shift value is not reliable in an ultra-low field. The relative Knight shift $\Delta K = K - K_0$, where K_0 is the average value above $T_{\rm c}$, has very weak dependence on field. The ΔK values for all directions are almost unchanged above $T_{\rm c}$ and decrease below $T_{\rm c}$, as shown in Fig. 3, which is consistent with spin-singlet pairing. The perturbing field is much larger than the lower critical field, so the drop below $T_{\rm c}$ is not from Meissner effect but intrinsic spin susceptibility.

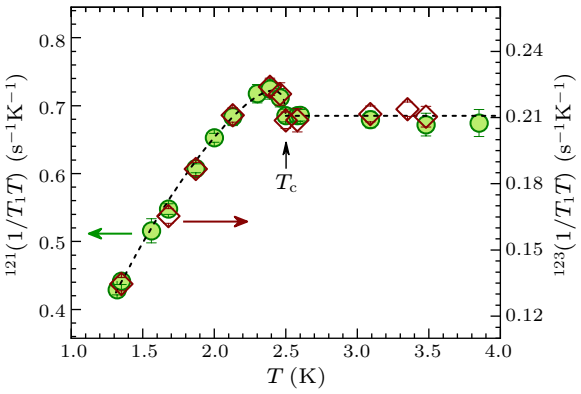

Fig. 4. Temperature dependence of $^{121}(1/T_1T)$ (left axis) and $^{123}(1/T_1T)$ (right axis). A Hebel–Slichter coherence peak appears just below $T_{\rm c}$. The curve and line are guides to the eyes.

In an ultra-low field, ^{121}K measurements have large errors which preclude further analysis. On the other hand, spin-lattice relaxation rate can be measured accurately. $^{121/123}(1/T_1T)$ shows a clear Hebel–Slichter coherence peak just below $T_{\rm c}$ and then rapidly decreases at low temperatures as shown in Fig. 4. It evidences that the superconducting gap is of s-wave symmetry. As for d- or p-wave, gap sign changes over the Fermi surface, which suppresses a coherence peak. In iron-based superconductors, $s^{\pm}$-wave also changes gap sign between different Fermi surfaces and suppresses a coherence peak.[37] So far, the Hebel–Slichter coherence peak has only been observed in s-wave superconductors. Here the coherence peak is small, which may be due to residual EFG fluctuations[38] and/or a strong electron-phonon coupling.[39] In other s-wave superconductors, the coherence peaks of Sb are also very small, such as in $YbSb_2$[40] and $BaTi_2Sb_2O$.[36] A recent STM study has suggested the absence of sign-change in the superconducting order parameter.[41] Magnetic penetration depth measured by tunneling diode oscillator has shown a nodeless behavior.[30] These results are both consistent with the s-wave gap symmetry. There is also experimentally observed residual density of states in the superconducting state,[25,41] which may be due to the competition between superconductivity and CDW. Another s-wave superconductor $Ta_4Pd_3Te_{16}$ also has a CDW order coexisting with superconductivity and shows residual density of states in the superconducting state.[42]

$^{121}(1/T_1T)$ is measured at the split peak due to the CDW transition and shows sudden changes at both $T_{\rm CDW}$ and $T_{\rm c}$, which indicates that the superconductivity coexists with the CDW state. The coexistence

of superconductivity and topological charge order may stimulate exotic excitations in the surface state,[26,43] which needs further investigations. Recently another superconducting phase at high pressure was found in CsV_3Sb_5.[24,25] Whether the high-pressure superconducting phase is the same as that at ambient pressure needs further studies.

In conclusion, we have performed ^{51}V NMR and $^{121/123}$Sb NQR studies on CsV_3Sb_5. The variation of the NMR and NQR spectra below T_{CDW} can be understood by the occurrence of a first-order commensurate CDW transition. EFG fluctuations are suppressed and magnetic fluctuations become dominant at low temperature. In the superconducting state, ^{121}K decreases and $^{121/123}(1/T_1T)$ shows a coherence peak just below T_c, which is the hallmark of the s-wave full gap superconductivity. The superconductivity coexists with the CDW state, which may lead to exotic surface state.

We thank S. K. Su, X. B. Zhou and B. Su for assistance in some of the measurements.

References

[1] Wang W S, Li Z Z, Xiang Y Y and Wang Q H 2013 *Phys. Rev. B* **87** 115135
[2] Kiesel M L, Platt C and Thomale R 2013 *Phys. Rev. Lett.* **110** 126405
[3] Yan S, Huse D A and White S R 2011 *Science* **332** 1173
[4] Fu M, Imai T, Han T H and Lee Y S 2015 *Science* **350** 655
[5] Khuntia P, Velazquez M, Barthélemy Q, Bert F, Kermarrec E, Legros A, Bernu B, Messio L, Zorko A and Mendels P 2020 *Nat. Phys.* **16** 469
[6] Guo H M and Franz M 2009 *Phys. Rev. B* **80** 113102
[7] Ko W H, Lee P A and Wen X G 2009 *Phys. Rev. B* **79** 214502
[8] Yu S L and Li J X 2012 *Phys. Rev. B* **85** 144402
[9] Ortiz B R, Gomes L C, Morey J R, Winiarski M, Bordelon M, Mangum J S, Oswald I W H, Rodriguez-Rivera J A, Neilson J R, Wilson S D, Ertekin E, McQueen T M and Toberer E S 2019 *Phys. Rev. Mater.* **3** 094407
[10] Ortiz B R, Teicher S M L, Hu Y, Zuo J L, Sarte P M, Schueller E C, Abeykoon A M M, Krogstad M J, Rosenkranz S, Osborn R, Seshadri R, Balents L, He J and Wilson S D 2020 *Phys. Rev. Lett.* **125** 247002
[11] Ortiz B R, Sarte P M, Kenney E M, Graf M J, Teicher S M L, Seshadri R and Wilson S D 2021 *Phys. Rev. Mater.* **5** 034801
[12] Yin Q W, Tu Z J, Gong C S, Fu Y, Yan S H and Lei H C 2021 *Chin. Phys. Lett.* **38** 037403
[13] Jiang Y X, Yin J X, Denner M M, Shumiya N, Ortiz B R, He J, Liu X, Zhang S S, Chang G, Belopolski I, Zhang Q, Hossain M S, Cochran T A, Multer D, Litskevich M, Cheng Z J, Yang X P, Guguchia Z, Xu G, Wang Z, Neupert T, Wilson S D and Hasan M Z 2020 arXiv:2012.15709 [cond-mat.supr-con]
[14] Yang S Y, Wang Y, Ortiz B R, Liu D, Gayles J, Derunova E, Gonzalez-Hernandez R, Šmejkal L, Chen Y, Parkin S S P, Wilson S D, Toberer E S, McQueen T and Ali M N 2020 *Sci. Adv.* **6** eabb6003
[15] Kenney E M, Ortiz B R, Wang C, Wilson S D and Graf M J 2021 *J. Phys.: Condens. Matter* **33** 235801
[16] Yu F H, Wu T, Wang Z Y, Lei B, Zhuo W Z, Ying J J and Chen X H 2021 arXiv:2102.10987 [cond-mat.str-el]
[17] Feng X, Jiang K, Wang Z and Hu J 2021 *Sci. Bull.* (in press)
[18] Denner M M, Thomale R and Neupert T 2021 arXiv:2103.14045 [cond-mat.str-el]
[19] Li H X, Zhang T T, Pai Y Y, Marvinney C, Said A, Yilmaz T, Yin Q, Gong C, Tu Z, Vescovo E, Moore R G, Murakami S, Lei H C, Lee H N, Lawrie B and Miao H 2021 arXiv:2103.09769 [cond-mat.supr-con]
[20] Zhou X, Li Y, Fan X, Hao J, Dai Y, Wang Z, Yao Y and Wen H H 2021 arXiv:2104.01015 [cond-mat.supr-con]
[21] Chen K Y, Wang N N, Yin Q W, Gu Y H, Jiang K, Tu Z J, Gong C S, Uwatoko Y, Sun J P, Lei H C, Hu J P and Cheng J G 2021 *Phys. Rev. Lett.* **126** 247001
[22] Du F, Luo S, Ortiz B R, Chen Y, Duan W, Zhang D, Lu X, Wilson S D, Song Y and Yuan H 2021 *Phys. Rev. B* **103** L220504
[23] Zhang Z, Chen Z, Zhou Y, Yuan Y, Wang S, Wang J, Yang H, An C, Zhang L, Zhu X, Zhou Y, Chen X, Zhou J and Yang Z 2021 *Phys. Rev. B* **103** 224513
[24] Chen X, Zhan X, Wang X, Deng1 J, Liu X B, Chen X, Guo J G and Chen X L 2021 *Chin. Phys. Lett.* **38** 057402
[25] Zhao C C, Wang L S, Xia W, Yin Q W, Ni J M, Huang Y Y, Tu C P, Tao Z C, Tu Z J, Gong C S, Lei H C, Guo Y F, Yang X F and Li S Y 2021 arXiv:2102.08356 [cond-mat.supr-con]
[26] Liang Z, Hou X, Ma W, Zhang F, Wu P, Zhang Z, Yu F, Ying J J, Jiang K, Shan L, Wang Z and Chen X H 2021 arXiv:2103.04760 [cond-mat.supr-con]
[27] Chen H, Yang H, Hu B, Zhao Z, Yuan J, Xing Y, Qian G, Huang Z, Li G, Ye Y, Yin Q, Gong C, Tu Z, Lei H, Ma S, Zhang H, Ni S, Tan H, Shen C, Dong X, Yan B, Wang Z and Gao H J 2021 arXiv:2103.09188 [cond-mat.supr-con]
[28] Wang Y, Yang S, Sivakumar P K, Ortiz B R, Teicher S M L, Wu H, Srivastava A K, Garg C, Liu D, Parkin S S P, Toberer E S, McQueen T, Wilson S D and Ali M N 2020 arXiv:2012.05898 [cond-mat.supr-con]
[29] Xu J P, Wang M X, Liu Z L, Ge J F, Yang X, Liu C, Xu Z A, Guan D, Gao C L, Qian D, Liu Y, Wang Q H, Zhang F C, Xue Q K and Jia J F 2015 *Phys. Rev. Lett.* **114** 017001
[30] Duan W, Nie Z, Luo S, Yu F, Ortiz B R, Yin L, Su H, Du F, Wang A, Chen Y, Lu X, Ying J, Wilson S D, Chen X, Song Y and Yuan H 2021 arXiv:2103.11796 [cond-mat.supr-con]
[31] Clark W G, Hanson M E, Lefloch F and Ségransan P 1995 *Rev. Sci. Instrum.* **66** 2453
[32] Ni S, Ma S, Zhang Y, Yuan J, Yang H, Lu Z, Wang N, Sun J, Zhao Z, Li D, Liu S, Zhang H, Chen H, Jin K, Cheng J, Yu L, Zhou F, Dong X, Hu J, Gao H J and Zhao Z 2021 *Chin. Phys. Lett.* **38** 057403
[33] Sakurai A, Matsumura M, Kato H, Nishioka T, Matsuoka E, Hayashi K and Takabatake T 2008 *J. Phys. Soc. Jpn.* **77** 063701
[34] Asayama K 2002 *Nuclear Magnetic Resonance in Itinerant Electron System* (Tokyo: Shokabo)
[35] Julien M H, Simonet V, Canals B, Ballou R, Hassan A K, Affronte M, Garlea V O, Darie C and Bordet P 2013 *Phys. Rev. B* **87** 214423
[36] Kitagawa S, Ishida K, Nakano K, Yajima T and Kageyama H 2013 *Phys. Rev. B* **87** 060510(R)
[37] Parker D, Dolgov O V, Korshunov M M, Golubov A A and Mazin I I 2008 *Phys. Rev. B* **78** 134524
[38] Li Z, Jiao W H, Cao G H and Zheng G Q 2016 *Phys. Rev. B* **94** 174511
[39] Kotegawa H, Ishida K, Kitaoka Y, Muranaka T and Akimitsu J 2001 *Phys. Rev. Lett.* **87** 127001
[40] Kohori Y, Kohara T, Sato N and Kinokiri T 2003 *Physica C* **388–389** 579
[41] Xu H S, Yan Y J, Yin R, Xia W, Fang S, Chen Z, Li Y, Yang W, Guo Y and Feng D L 2021 arXiv:2104.08810 [cond-mat.supr-con]
[42] Pan J, Jiao W H, Hong X C, Zhang Z, He L P, Cai P L, Zhang J, Cao G H and Li S Y 2015 *Phys. Rev. B* **92** 180505
[43] Fu L and Kane C L 2008 *Phys. Rev. Lett.* **100** 096407

Supplemental Material for "**S-Wave Superconductivity in Kagome Metal CsV_3Sb_5 Revealed by $^{121/123}$Sb NQR and ^{51}V NMR Measurements**

Chao Mu,[1, 2] Qiangwei Yin,[3] Zhijun Tu,[3] Chunsheng Gong,[3] Hechang Lei,[3] Zheng Li,[1, 2,] and Jianlin Luo[1, 2, 4]
[1]Beijing National Laboratory for Condensed Matter Physics and Institute of Physics, Chinese Academy of Sciences, Beijing 100190, China
[2]School of Physical Sciences, University of Chinese Academy of Sciences, Beijing 100190, China
[3]Department of Physics and Beijing Key Laboratory of Opto-electronic Functional Materials & Micro-nano Devices, Renmin University of China, Beijing 100872, China
[4]Songshan Lake Materials Laboratory, Dongguan 523808

1. Knight shift and spin-lattice relaxation rate of ^{51}V with $H \perp c$

Figure S1 shows ^{51}K jumps up below T_{CDW} with $H \perp c$, however $^{51}(1/T_1T)$ for both directions does not jump up. It indicates that the splitting and jumping of ^{51}K at T_{CDW} are not by the change of hyperfine coupling constants, but by the orbital part of Knight shift.

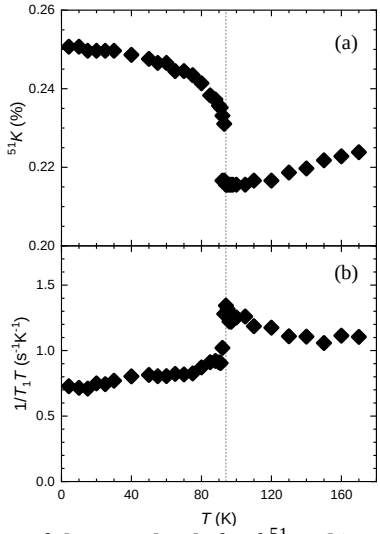

Fig. S1. (a) Temperature dependence of the Knight shift of ^{51}V. (b) Temperature dependence of the $^{51}(1/T_1T)$. The vertical dashed line indicates the position of T_{CDW}.

2. Sb spectra

There are two different crystallographic sites of Sb in CsV_3Sb_5. Sb1 atoms locate in the kagome plane with V atoms and Sb2 atoms encapsulate the kagome layer with a graphitelike network. The atomic ratio is Sb1 : Sb2 = 1 : 4, which determines the spectra intensity ratio. Therefore, we can distinguish two Sb spectra by their peak intensity. Fig. S2 shows the spectrum from 67 MHz to 161 MHz at 4.2 K.

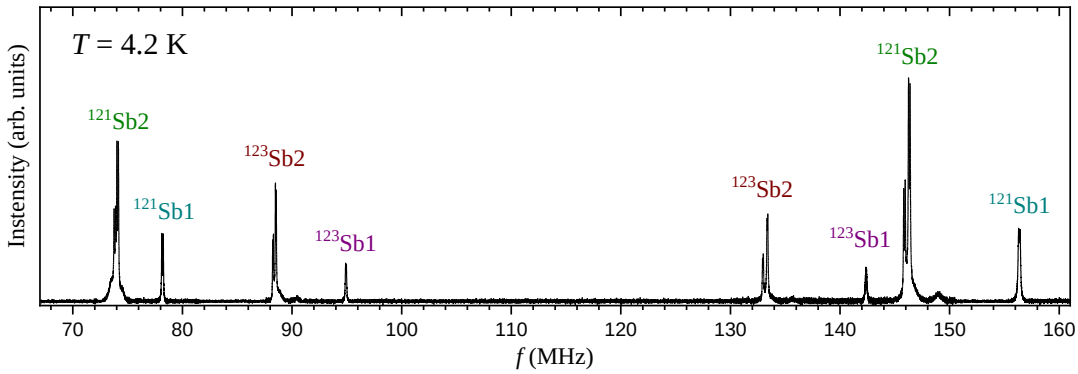

Fig. S2. $^{121/123}$Sb-NQR spectra with a perturbing field of 64 Oe along c-axis at 4.2 K.

The peaks of Sb1 atoms are shown in Fig. S3. Below T_{CDW} = 94 K, peaks shift to higher frequency which indicates EFG strength increases. The pairing of peaks at 4.2 K is due to a perturbing field of 64 Oe along *c*-axis. They merge together when peaks are broad at 130 K.

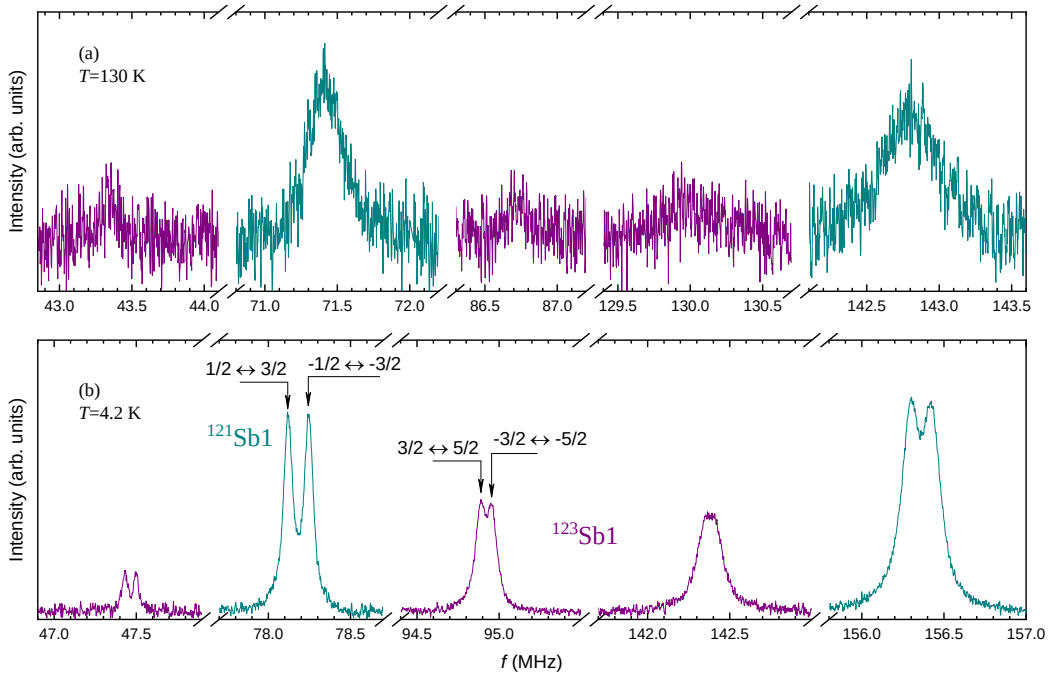

Fig. S3. (Color online) $^{121/123}$Sb1-NQR spectra with a perturbing field of 64 Oe along *c*-axis at (a) 130 K and (b) 4.2 K, respectively.

The change of EFG is different between Sb1 site and Sb2 sites below T_{CDW}. The EFG strength is enhanced without asymmetry at Sb1 site in the kagome plane. On the other hand, the main change is not the EFG strength, but the EFG direction at Sb2 sites out of kagome plane. Moreover, in the CDW state, Sb2 has two unequal sites with ratio of 1:2 from the electric field gradient point of view, while Sb1 has only one site. It imposes constraints on the possible configurations of the CDW state.

We emphasize that two Sb2 sites with ratio of 1:2 are intrinsic. There is only one set of peaks of Sb2 above T_{CDW} and no other peak from impurity. Below T_{CDW}, the peaks of Sb2 split into two sets, which is same as that of ^{51}V. The peaks of Sb1 do not split below T_{CDW}, as shown in Fig. S3 (b), so the splitting of Sb2 is not from defects. Otherwise, both Sb1 and Sb2 should split at the same time. The ratio of 1:2 is also an indirect proof that it is intrinsic. Defects induced peaks should have an arbitrary ratio and the ratio should change with temperature. Moreover, the full width at half maximum (FWHM) of two splitting peaks are same, which proves they are all intrinsic.